Fusion Technology

ISSN: 0748-1896 (Print) (Online) Journal homepage: http://www.tandfonline.com/loi/ufst19

Assessment of a Compact Torsatron Reactor, ATFSR

Wayne A. Houlberg, James T. Lacatski & Nermin A. Uckan

To cite this article: Wayne A. Houlberg, James T. Lacatski & Nermin A. Uckan (1986) Assessment of a Compact Torsatron Reactor, ATFSR, Fusion Technology, 10:2, 227-235, DOI: 10.13182/FST86-A24974

To link to this article: https://doi.org/10.13182/FST86-A24974

Published online: 09 May 2017.

ASSESSMENT OF A COMPACT TORSATRON REACTOR, ATFSR

FUSION REACTORS

WAYNE A. HOULBERG *Oak Ridge National Laboratory*
P.O. Box Y, Building 9201-2, MS-3, Oak Ridge, Tennessee 37831

JAMES T. LACATSKI* *University of Tennessee*
Nuclear Engineering Department, Knoxville, Tennessee 37917

NERMIN A. UCKAN *Oak Ridge National Laboratory*
P.O. Box Y, Building 9201-2, MS-3, Oak Ridge, Tennessee 37831

Received January 2, 1986
Accepted for Publication April 17, 1986

Confinement and engineering issues of a small (average minor radius $\bar{a} \simeq 1$ m) moderate-aspect-ratio torsatron reactor are evaluated. The Advanced Toroidal Facility design is used as a starting point because of its relatively low aspect ratio and high beta capabilities. The major limitation of the compact size is the lack of space under the helical coils for the blanket and shield. Some combination of lower aspect ratio coils, higher coil current density, thinner coils, and more effective shielding material under the coils should be incorporated into future designs to improve the feasibility of small torsatron reactor concepts. Current neoclassical confinement models for helically trapped particles show that a large radial electric field (in terms of the electric potential, $e\phi/T \geq 3$) is necessary to achieve ignition in a device of this size.

I. INTRODUCTION

Stellarator/torsatron reactors have the advantage of operating with zero net plasma current and steady-state magnetic fields, thus greatly reducing cyclic stresses and fatigue. Other advantages are disruption-free operation, natural divertor capabilities, startup on existing magnetic surfaces, and possible modular construction. Torsatrons have the additional advantage of improved access (relative to stellarators) because they require only l helical windings to produce a poloidal harmonic of l, as opposed to $2l$ windings in a stellarator. Reactor-relevant issues addressed here are the same as those for other magnetic confinement concepts: plasma beta (efficient use of the magnetic fields), engineering (size, access, shielding, etc.), and energy confinement (ignition versus high-Q operation).

The Advanced Toroidal Facility (ATF) torsatron[1] under construction at Oak Ridge National Laboratory (ORNL) should give direct access to the second stability regime (high beta) because of its moderate aspect ratio, its shear, and the stabilizing influence of the magnetic axis shift.[2] The lower aspect ratio of the ATF in combination with higher beta capabilities should lead to reactors that are more compact than those considered in earlier power reactor studies.[3-8] Parameters for these designs are listed in Table I and compared with the result of this study,[9] the ATF Stellarator Reactor (ATFSR). Reduced-aspect-ratio stellarators have been investigated in a parameter study by Hitchon.[10] Aspect ratios as low as $A \simeq 6.5$ were found, but constraints on the blanket/shield thickness led to minimum major radii of $R_0 \simeq 11$ m. In this study, we relax the blanket/shield constraint (but recognize it as a potential problem area) to obtain an even smaller device that falls into the category of an ignition machine. We devote greater attention to evaluation of confinement, which also plays a major role in minimum size projections but has been largely overlooked in previous studies.

We start with ATF, scale it up to an average plasma minor radius of $\bar{a} = 1$ m, then examine the confinement and engineering issues that have an impact on feasibility. In Sec. II the ATF magnetic field and magnetohydrodynamic (MHD) properties are summarized and scaled up for the ATFSR. Recently developed theoretical models[11] and experiments[12] on Wendelstein VII-A have shown the importance of a radial electric field for confinement. The transport equations and models, including the electric field evaluation, are presented in Sec. III, and the results are discussed in Sec. IV.

*Current address: Duke Power Company, Charlotte, North Carolina 28242.

TABLE I

Stellarator/Torsatron Power Reactor Designs

	Massachusetts Institute of Technology T-2	Japan Heliotron-H	Soviet Union TNPP	University of Wisconsin UWTOR-M	Los Alamos National Laboratory MSR-IIB	ORNL ATFSR
Plasma radius (m)	1.5	1.7	2.1	1.72	0.81	1.0
Major radius (m)	24.0	21.0	36.8	24.1	23.0	7.0
Aspect ratio	16.0	12.4	17.5	14.0	28.4	7.0
Plasma volume (m^3)	1067	1198	3203	1407	298	138
Average density ($10^{20}/m^3$)	2.5	1.17	2.5	1.46	3.64	1.2
Average beta	0.065	0.06	0.1	0.06	0.08	0.09
On-axis magnetic field (T)	5.0	4.0	4.4	4.5	6.56	5.0
Peak field at coil (T)	9.0	9.0		11.6	11.6	10.0
First-wall loading (MW/m^2)	2.2	1.3	4.0	1.41	2.0	2.3
Thermal power [MW(thermal)]	3600	3400	9300	4820	4000	930
Net plant efficiency	0.33	0.31	0.36	0.38	0.33	0.33
Net electric power [MW(electric)]	1188	1054	3348	1832	1320	300

II. MAGNETIC PROPERTIES OF ATF AND ATFSR

The ATF torsatron is an $l = 2$ (two helical coils), $m = 12$ [12 toroidal field (TF) periods] design with additional inner, middle, and outer vertical field (VF) coils, as shown in Fig. 1. For confinement studies, the magnetic field strength can be approximated as

$$B \simeq B_0[1 - \epsilon_t \cos\theta - \epsilon_h \cos(l\theta - m\phi)] \ , \qquad (1)$$

where the toroidal modulation is given by the local inverse aspect ratio $\epsilon_t \simeq \rho/R_0$ and the helical modulation is

$$\epsilon_h \simeq \epsilon_{h0} + \epsilon_{ha}(\rho/\bar{a})^2 \ , \qquad (2)$$

with $0 \le \rho \le \bar{a}$. Table II summarizes the dimensionless machine parameters that ATF and ATFSR have in

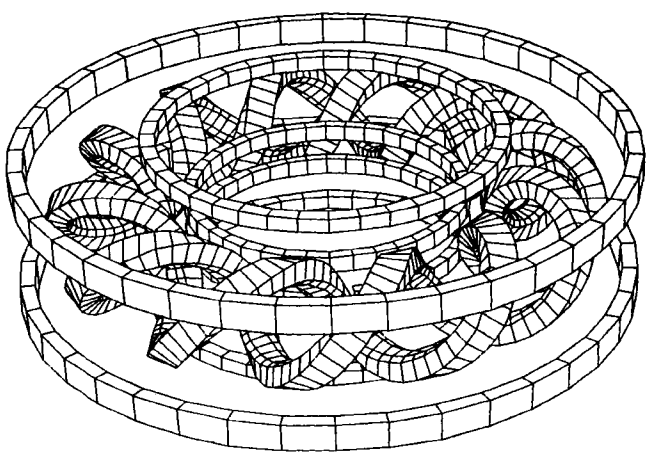

Fig. 1. The ATF-style coil set. The inner, middle, and outer VF coils are shown. The middle VF coil system (upper coils inside torus) adds flexibility to the ATF configuration but can be eliminated in ATFSR.

TABLE II

ATF and ATFSR Machine Parameters

Dimensionless Parameters	
Coil configuration	Continuous
Multipolarity, l	2
TF periods, m	12
Plasma elongation, b_p/a_p	1.65
Plasma aspect ratio, $R_0/\bar{a}$	7
Coil aspect ratio, $R_0/\bar{a}_c$	4
Helical ripple on axis, ϵ_{h0}	0.0
Helical ripple at edge, ϵ_{ha}	0.22
Transform on axis, ι_0	0.35
Transform at edge, ι_a	0.90

Scaled Parameters	ATF	ATFSR
Major radius, R_0 (m)	2.1	7.0
Average minor radius, $\bar{a}$ (m)	0.3	1.0
Plasma minor radius, a_p (m)	0.23	0.78
Average coil radius, a_c (m)	0.48	1.75
Major radius of inner VF coils (m)	1.33	4.43
Major radius of outer VF coils (m)	2.94	9.80
Major radius of middle VF coils (m)[a]	1.69	
Vertical position of inner VF coils (m)	±0.20	±0.67
Vertical position of outer VF coils (m)	±0.64	±2.13
TF on axis, B_0 (T)	2.0	5.0
Helical coil current (MA)	1.75	14.6

[a]Middle VF coils are used to add flexibility to the ATF magnetic configuration. The standard configuration requires no current in these coils.

common and also the scaled sizes, fields, and currents. For ATFSR, the size has been scaled up by a factor of 10/3 and the magnetic field by a factor of 5/2; coil currents must be scaled by the product of these two factors, or 25/3, according to Ampère's law.

One of the most appealing aspects of the ATF configuration is its MHD stability properties,[1,2] as shown in Fig. 2. The equilibrium limit has been extended to slightly higher beta than that shown through improved resolution in the computational models. The limit corresponds to a constraint that the Shafranov shift be less than ~50% of the minor radius. The stability boundary is determined by low-n, internal ideal instabilities near the plasma edge, which is bounded by a close-fitting conducting shell. As the shell is moved away from the plasma, no significant change is seen in this boundary. In the standard ATF configuration, resistive modes are expected to occur only in the edge region. Saturation of the modes leads to turbulence and enhanced transport (e.g., resistive-g modes). The ATF has enough flexibility in its helical field (HF) and VF coil systems to examine whether the window to the second stability regime exists and, if it does exist, to attempt to optimize the magnetic configuration. The equilibrium and stability limits of Fig. 2 should apply directly to ATFSR because the same magnetic configuration is used. An average beta of 9% has been chosen for the reference operating point of ATFSR, although there is a large uncertainty in this number as an upper limit on beta.

The one major problem in scaling up the ATF design is the rather tight area between the plasma and the HF coils, $\Delta S \simeq 0.4$ m, as shown schematically in Fig. 3 (dimensions and other parameters are given in Table III). A 0.1-m dewar and a 0.05-m first-wall thickness are assumed. Because ATF was not designed to allow for a blanket/shield, it is not surprising that a simple scale-up of the device leads to limited space in this region. If ΔS can be increased to 0.6 to 0.7 m, however, an efficient shielding material, such as tungsten with boron carbide, could be used directly under the coils.[13]

In tokamak plasmas, where very low order harmonics of the poloidal magnetic field are used for shaping, it is relatively easy to move the coils (in minor radius) away from the plasma and allow for a thicker blanket/shield. In stellarators or torsatrons, even small modifications to the HF coils can have a significant effect on the vacuum magnetic field topology. Nonetheless, several options to relax the tight spacing of the ATF scale-up exist: thinner, higher current density coils with the same height and aspect ratio (i.e., the same distance from the coil center to the plasma); lower aspect ratio HF coils; a larger scale device; or some combination of these. Changing either the aspect

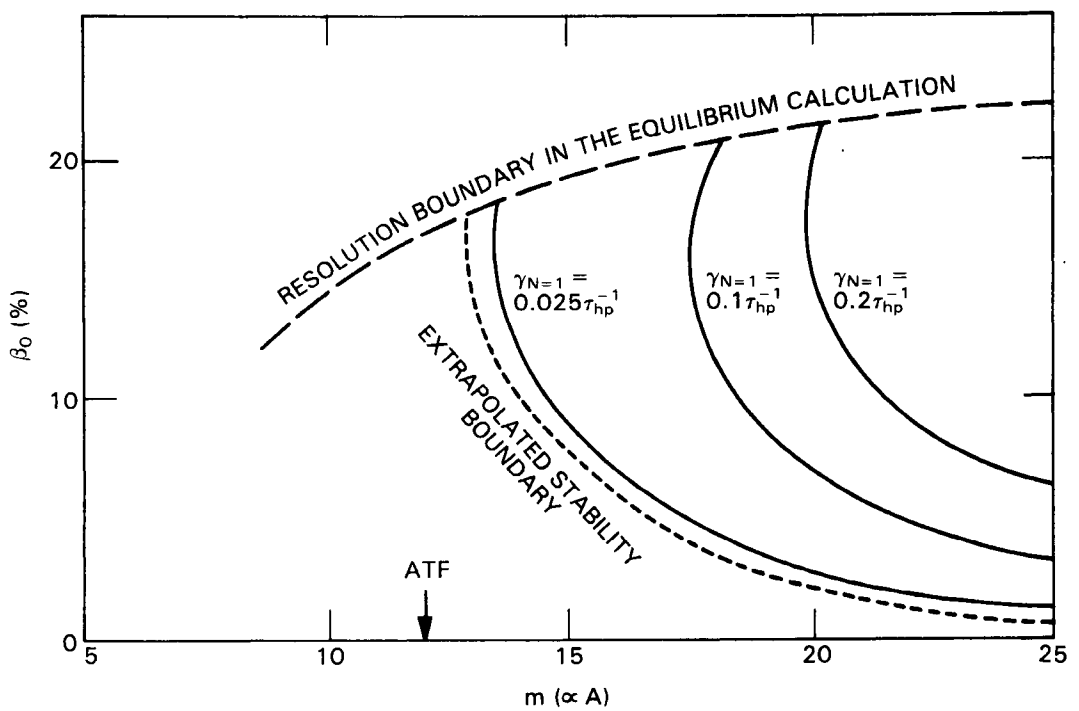

Fig. 2. Combined equilibrium and stability constraints for ATF, showing central β_0 as a function of TF period number. These constraints indicate possible access to the second stability regime at $m = 12$.

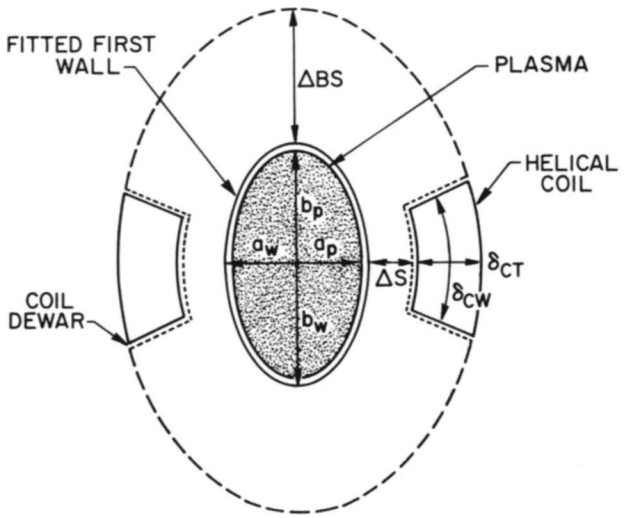

Fig. 3. Schematic cross-sectional view of ATFSR, showing the elliptic plasma (semiminor radius a_p, semimajor radius b_p) with a fitted first wall (semiminor radius a_w, semimajor radius b_w) a coil shield (thickness ΔS), and a blanket (blanket/shield thickness ΔBS). The coil dewars and the HF coils (thickness δ_{CT}, width δ_{CW}) are shown with the cross sections normal to the coils; the projections of their cross sections in this plane are larger than shown because of the helical pitch of the coils. The plasma chamber rotates poloidally with the TF period number $m = 12$.

TABLE III

ATFSR Blanket, Shield, and Coil Parameters

First-wall configuration	Fitted
Wall semiminor radius, a_w (m)	0.86
Wall semimajor radius, b_w (m)	1.37
Wall surface area, S_w (m^2)	276
First-wall thickness (m)	0.05
Dewar thickness (m)	0.1
Coil shield thickness, ΔS (m)	0.4
Blanket/shield thickness, ΔBS (m)	1.5
Field at coil, B_{max} (T)	10
Maximum current density (MA/m^2)	15
Coil thickness, δ_{CT} (m)	0.7
Coil width, δ_{CW} (m)	1.4

ratio or the dimensions of the HF coils requires reassessment of the magnetics and a more thorough study than that undertaken here. Lower aspect ratio coil designs that preserve the desirable MHD characteristics of ATF are under investigation.[14]

The HF coils in ATF are designed for 28 MA/m^2 in the copper or ~20 MA/m^2 averaged over the coil, including structure and cooling channels. The scale-up to ATFSR leads to a reduction in HF coil current density to ~15 MA/m^2. The field at the coil is twice that on axis, $B_c \simeq 10$ T, so the design is comfortably within the limits for pool boiling in NbTi superconductor magnets (≃18 to 20 MA/m^2). Forced flow in Nb_3Sn could raise the limit to ≃40 MA/m^2 (Ref. 15).

The chamber wall is shown as fitted to the plasma in Fig. 3. Because space is not a restriction in the semimajor radius (located at the top and bottom in the figure, and rotating poloidally as it moves toroidally around the machine), room can be made for an expanded boundary or divertor[16] to collect particles and energy; for diagnostic, fueling, and heating ports; etc.

III. CONFINEMENT MODEL WITH RADIAL ELECTRIC FIELD EFFECTS

The confinement properties of ATFSR were examined with the POPCON option in the WHIST transport code,[17] including the analysis of Hastings et al. for a neoclassical formulation of the radial electric field.[11] The particle and energy transport equations are essentially those used in tokamak analyses, but with the radial electric field effects incorporated into the radial fluxes.

The particle balance is given by

$$\frac{\partial}{\partial t} n_a + \frac{1}{V'(\rho)} \frac{\partial}{\partial \rho} [V'(\rho)\Gamma_a] = S_{pa} \ , \qquad (3)$$

where

subscript a = any of the ion species

$V(\rho)$ = volume of plasma contained inside the flux surface ρ

$V'(\rho)$ = effective surface area of the flux surface ρ.

The particle source represents the net source of ions from all atomic physics processes. Pellet fueling is taken as the source of deuterium and tritium in the ATFSR calculations. The electron density is treated as a dependent variable and evaluated from charge neutrality.

The energy balance for ions results from a summation over all thermal ion species, using the assumption that strong collisional coupling equilibrates their temperatures at T_i:

$$\frac{3}{2} \frac{\partial}{\partial t} \left[\left(\sum_a n_a \right) T_i \right] + \sum_a \left\{ \frac{1}{V'(\rho)} \frac{\partial}{\partial \rho} \left[V'(\rho) \left(q_a + \frac{5}{2} \Gamma_a T_i \right) \right] \right\} = \sum_a \left[\frac{\Gamma_e}{n_e} \frac{\partial}{\partial \rho} (n_a T_i) + Q_{ea} + S_{Ea} - Z_a \Gamma_a \phi' \right] , \qquad (4)$$

where the right side of Eq. (4) contains, in order, the flow-work term, the energy exchange between the electron and ion fluids, the heating of thermal ions from both external (e.g., wave heating, beam injection) and internal (e.g., energetic fusion-produced alphas) sources, and the kinetic energy expended (created) by the ions in climbing (falling) through the radial electric potential.

The electron energy balance equation is notationally the same as the ion energy balance with the subscript e replacing a, the species summation removed on the left side, and the sign changed on the flow-work and energy exchange terms:

$$\frac{3}{2}\frac{\partial}{\partial t}(n_e T_e) + \frac{1}{V'(\rho)}\frac{\partial}{\partial \rho}\left[V'(\rho)\left(q_e + \frac{5}{2}\Gamma_e T_e\right)\right] = -\sum_a \left[\frac{\Gamma_e}{n_e}\frac{\partial}{\partial \rho}(n_a T_i) + Q_{ea}\right] + S_{Ee} + \Gamma_e \phi' \ , \quad (5)$$

where radiative losses are included in the electron energy source term, in addition to the energy sources discussed in the ion energy equation.

The particle and heat fluxes are assumed to consist of three parts: a neoclassical contribution from particles trapped in the helical ripple (*ncr*), a neoclassical axisymmetric contribution (*nca*) from toroidally trapped particles, and an additional anomalous term (*an*) where warranted by experimental evidence. Thus,

$$\Gamma_j = \Gamma_j^{ncr} + \Gamma_j^{nca} + \Gamma_j^{an} \quad (6)$$

and

$$q_j = q_j^{ncr} + q_j^{nca} + q_j^{an} \ , \quad (7)$$

where the subscript j designates either ions or electrons.

The integral formulation of Shaing[18] gives a smooth fit to the neoclassical particle and energy fluxes of helically trapped ions and electrons over a wide range of plasma parameters. The particle fluxes are given by

$$\Gamma_j^{ncr} = -\epsilon_t^2 \epsilon_h^{1/2} \nu_{dj}^2 n_j \int_0^\infty dx\, x^{5/2} e^{-x} \tilde{\nu}_j(x) \frac{A_j(x)}{\omega_j^2(x)} \ . \quad (8)$$

The drift of species j in the nonuniform magnetic field is

$$\nu_{dj} \equiv \frac{T_j}{Z_j e B \rho} \ . \quad (9)$$

The effective collisionality in the helical magnetic field is

$$\tilde{\nu}_j(x) \equiv \frac{\nu_j(x)}{\epsilon_h} \ , \quad (10)$$

where ν_j is the energy-dependent 90-deg collision frequency; the dimensionless energy is

$$x \equiv \frac{m_j v_{thj}^2}{2 T_j} \ ; \quad (11)$$

and the expressions for ϵ_t and ϵ_h are given in Sec. II. The driving forces for the fluxes are radial nonuniformities in the fluid quantities (assumed constant on a magnetic surface):

$$A_j(x) \equiv \frac{1}{n_j}\frac{\partial n_j}{\partial \rho} + \frac{Z_j e}{T_j}\frac{\partial \phi}{\partial \rho} + \frac{1}{T_j}\left(x - \frac{3}{2}\right)\frac{\partial T_j}{\partial \rho} \ . \quad (12)$$

The effective frequency in the denominator of the integrand of Eq. (8) is given by

$$\omega_j^2 \equiv \omega_{dj}^2 + \omega_{sj}^2 + \omega_{pj}^2 + \omega_{\nu j}^2 \ , \quad (13)$$

where the electric field and grad-B drift contribute to an effective drift frequency in the collisionless nonresonant regime,

$$\omega_{dj}^2 \equiv 1.67 \frac{\epsilon_t}{\epsilon_h}(\omega_E + \omega_{\nabla Bj})^2 \ , \quad (14)$$

with

$$\omega_E \equiv -\frac{\phi'}{eB\rho} \quad (15)$$

and

$$\omega_{\nabla Bj} \equiv -x\nu_{dj}\frac{\partial \epsilon_h}{\partial \rho} \ . \quad (16)$$

The superbanana, plateau, and collisional terms are obtained with the following effective frequencies:

$$\omega_{sj}^2 \equiv 0.25\left(\frac{\epsilon_t}{\epsilon_h}\right)^{3/2}\omega_{\nabla Bj}^2 \ , \quad (17)$$

$$\omega_{pj}^2 \equiv 0.6|\omega_{\nabla Bj}|\frac{\nu_j(x)}{\epsilon_h} \ , \quad (18)$$

and

$$\omega_{\nu j}^2 \equiv 3.0\left[\frac{\nu_j(x)}{\epsilon_h}\right]^2 \ , \quad (19)$$

respectively.

The neoclassical heat fluxes for ripple-trapped ions and electrons are similar to the neoclassical particle fluxes but involve a higher velocity moment of the distribution function:

$$Q_j^{ncr} = q_j^{ncr} + \frac{5}{2}\Gamma_j^{ncr} T_j = -\epsilon_t^2 \epsilon_h^{1/2} \nu_{dj}^2 n_j T_j^2 \int_0^\infty dx\, x^{7/2} e^{-x} \tilde{\nu}_j(x) \frac{A_j(x)}{\omega_j^2(x)} \ . \quad (20)$$

The integrals over velocity space in Eqs. (12) and (20) are evaluated numerically. The axisymmetric neoclassical terms are taken from Hinton and Hazeltine[19] in simplified diagonal form.

In the collisional regime of existing experiments, the neoclassical particle and electron heat fluxes are small and, therefore, susceptible to anomalous transport because of small-scale turbulence, as in tokamak plasmas. An additional contribution is typically added to the neoclassical fluxes for better experimental agreement.[20] We add the following anomalous terms to the

particle and electron heat fluxes, assuming (for lack of a better understanding of the physical processes involved) that the contributions to the electron and ion particle fluxes are equal and do not influence the radial potential:

$$\Gamma_j^{an} = \Gamma_j - \Gamma_j^{nc} = -D^{an}\frac{\partial n_e}{\partial \rho} \quad (21)$$

and

$$q_e^{an} = -n_e \chi_e^{an}\frac{\partial T_e}{\partial \rho} \ , \quad (22)$$

where

$$D^{an} = \chi_e^{an}/3 = \frac{1.5\times 10^{12}}{n_e} \quad (\mathrm{m^2/s}) \ . \quad (23)$$

Two methods of incorporating the radial electric field are discussed in the following analysis: (a) assuming a parabolic profile for the electric potential normalized to the central ion temperature,

$$\phi = -\xi T_i(0)\left(\frac{\rho}{\bar{a}}\right)^2 \ , \quad (24)$$

and (b) solving for a self-consistent radial electric potential from the neoclassical particle fluxes.

In an axisymmetric tokamak plasma, the radial electric field term is ignored, using the argument that the radial fluxes of ions and electrons are intrinsically ambipolar. In a nonaxisymmetric plasma, the radial electric field ($-\phi'$) strongly influences the particle drifts and, therefore, the net particle fluxes. The constraint that the radial charge flows of electrons and ions must be equal then leads to an algebraic equation for the radial electric field that is highly nonlinear and multivalued for neoclassical transport models[21,22]:

$$\Gamma_e(\rho,\phi') = \sum_a Z_a \Gamma_a(\rho,\phi') \ . \quad (25)$$

Because of the assumption that the axisymmetric and anomalous contributions are independent of ϕ', Eq. (25) reduces to

$$\Gamma_e^{ncr}(\rho,\phi') = \sum_a Z_a \Gamma_a^{ncr}(\rho,\phi') \ . \quad (26)$$

Time evolution of the electric field can lead to discontinuities in the radial solution,[23] so we adopt a diffusion equation for the evolution of ϕ' rather than using Eq. (26) (Refs. 11 and 24):

$$\frac{\partial}{\partial t}\left[\epsilon_0 \frac{c^2}{v_{Ap}^2}\left(\frac{1}{q}\right)\phi'\right] = \sum_j \left\{ Z_j e \Gamma_j^{ncr} + \frac{1}{V'(\rho)}\frac{\partial}{\partial \rho} \times \left[V'(\rho) Z_j D_{Ej} \frac{\partial \phi'}{\partial \rho}\right]\right\} \ , \quad (27)$$

where

$$D_{Ej} \equiv \frac{Z_j e}{T_j}\frac{3}{16\sqrt{2\pi}}\frac{n_j \nu_{thj} T_j^4}{(Z_j e)^4}\frac{\epsilon_t^4}{\sqrt{\epsilon_h}}\left(1+\frac{\epsilon_h}{\epsilon_t}\right) \times \int_{\tilde{x}_1}^{\infty} dx\, e^{-x}\frac{x^3}{|\phi'| + |x(T_j/Z_j e)\epsilon_h'|} \ , \quad (28)$$

$$\tilde{x}_1 \equiv \left\{\frac{\nu_{thj}}{\epsilon_h[|\phi'| + |(T_j/Z_j e)\epsilon_h'|]}\right\}^{2/3} \ , \quad (29)$$

and v_{Ap} is the poloidal Alfvén velocity.

In steady state and in the absence of a very sharp gradient in ϕ [i.e., a discontinuity produced by the vanishing of a root of Eq. (26)], the solution of Eq. (27) reduces to that of Eq. (26). The time scale for this relaxation is faster than the particle or energy diffusion time scales, so an inner loop with a shorter time step is used to evolve this equation.

IV. DISCUSSION OF CONFINEMENT RESULTS

A Gaussian heating profile with a half-width of $\bar{a}/2$ and with 25% of the power delivered to the electrons and 75% to the thermal ions was used to simulate ion cyclotron resonant heating (ICRH) in the evaluation of auxiliary power needs for startup. Pellet fueling maintained equal densities of deuterium and tritium through feedback on the source.

Figure 4 shows the operating contours (in $\langle n_e\rangle$-$\langle T\rangle$ space) for a fixed potential characterized by $\xi = 4$, where

$$\langle T\rangle \equiv \frac{1}{\langle n_e\rangle}\frac{1}{2V}\int dV (n_e T_e + n_i T_i) \quad (30)$$

and $\langle n_e\rangle$ is the volume-averaged electron density. Ignition ($P_{aux}^{eq} = 0$) occurs at $\langle\beta_T\rangle \simeq 8\%$ with a fusion power output of ~300 MW. The reference operating values of Table I are obtained at the intersection of the ignition curve and the $\langle\beta_T\rangle = 9\%$ contour. A recirculating power fraction of 5%, a thermal conversion efficiency of 33%, and an energy multiplication factor of 1.2 in the blanket have also been assumed. The electron energy confinement time is ~0.5 s, and the ion energy confinement is ~5 s for a net global energy confinement time of 0.9 s—comparable to that for a tokamak of the same size.

Because stellarators can operate in a steady state, startup is infrequent, and there is no strong limitation on the startup time; the minimum in the steady-state auxiliary power contours between the origin ($\langle\beta_T\rangle = 0$) and the ignition curve then closely approximates the startup power requirements.[17] In this case, ~20 MW is required for a low-density startup.

The same analysis with $\xi = 2$ raises the ignition curve above 9% beta. For this case, $Q \simeq 15$ at the reference operating point, which requires ~50 MW of steady-state auxiliary power and has a global energy confinement time of ≃0.7 s. At $\xi \simeq 3$, the ignition

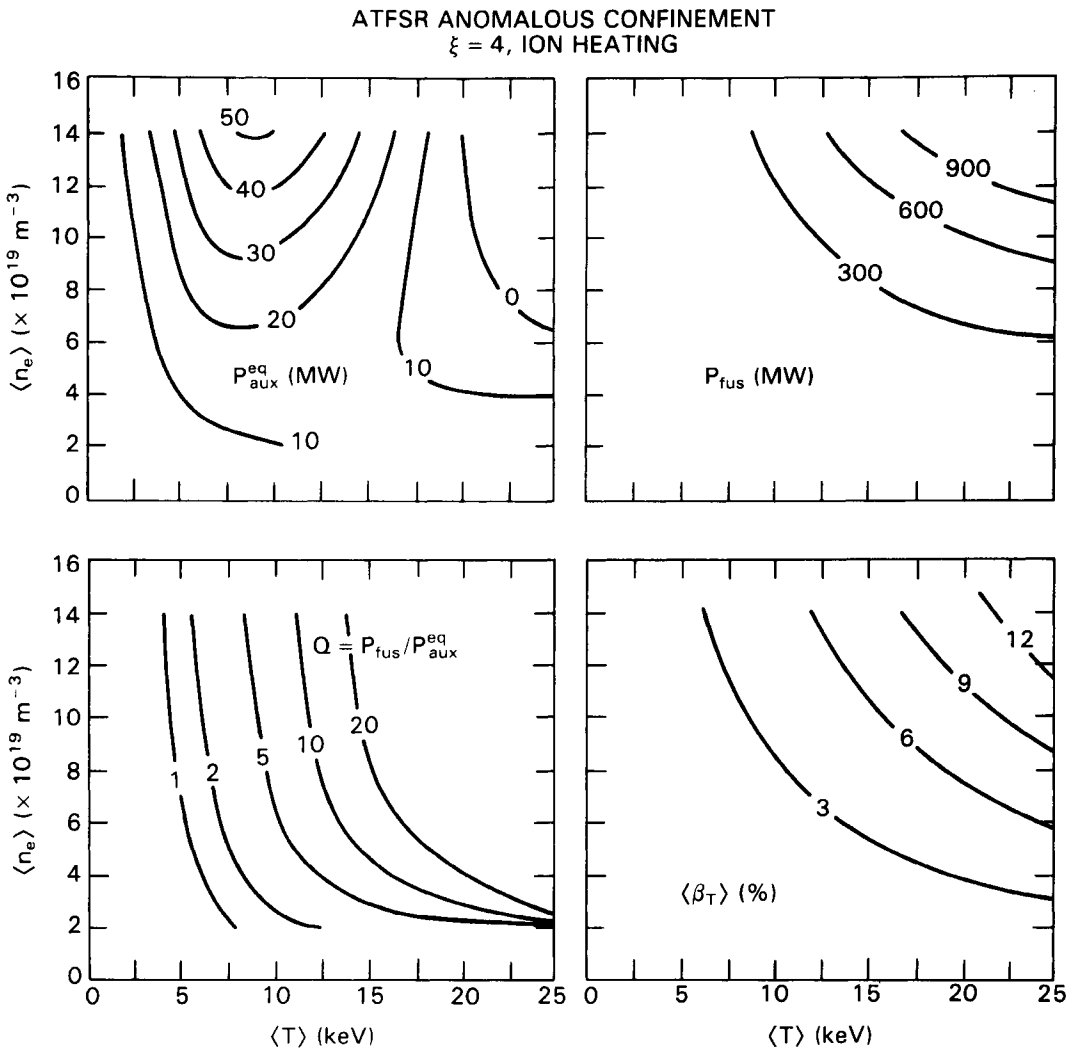

Fig. 4. Steady-state contours for an assumed electric potential profile characterized by $\xi = 4$. The contours are supplementary heating (P^{eq}_{aux}), fusion power (P_{fus}), Q (P_{fus}/P^{eq}_{aux}), and toroidal beta ($\langle\beta_T\rangle$).

curve just intersects the 9% beta curve, giving a single-point operating window (ignition margin of one).

At low temperatures, the neoclassical ion particle losses dominate and yield a negative ambipolar electric potential in the solution of Eq. (26) or (27). In the higher temperature, lower collisionality regime of a reactor, the electron losses dominate and a positive potential is obtained. This leads to a necessary transition through small potentials and electric fields where resonant neoclassical helical ripple losses are large. When Eq. (27) is solved through the transition zone, the results in Fig. 5 are obtained. The potential is forced to asymptotically approach $\xi = 4$ at high temperatures where the neoclassical ripple-induced fluxes are reduced and, therefore, are more vulnerable to anomalous losses. The $\phi = 0$ transition occurs along a curve roughly intersecting the bottoms of the auxiliary power contours and strengthens the requirement of a low-density startup. At a density of $\langle n_e\rangle \simeq 2 \times 10^{19}$ m^{-3}, an auxiliary power of $\simeq$20 MW (contour not shown) can be used to force the transition to the low-collisionality, electron-dominated loss solution at a low temperature ($\simeq$5 keV) where the conduction losses are not very severe. As the density is increased, the transition occurs at higher temperatures, with the resonant losses increasing rapidly.

V. SUMMARY

Emphasis has been placed in this study on a low-aspect-ratio torsatron configuration that has high beta capabilities and, thus, leads to an attractive reactor regime. The ATFSR represents only a preliminary scale-up of the ATF to a reactor that is more compact than those considered in earlier studies. Blanket/shield

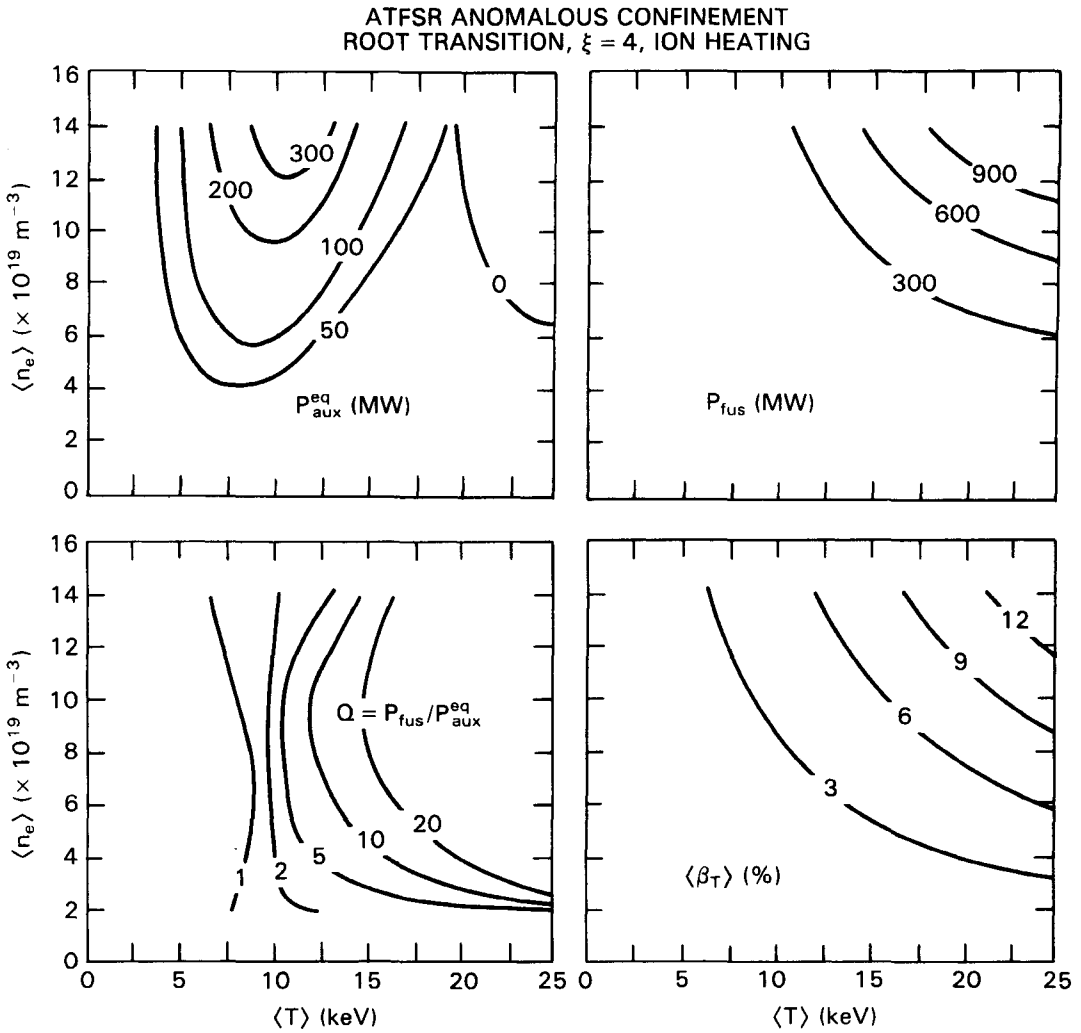

Fig. 5. Steady-state contours with self-consistent E_r evolution through the transition and $\xi = 4$ thereafter. The contours are those described in Fig. 4.

space under the helical coils is not adequate, but a push to helical coils with a slightly lower aspect ratio (from $\simeq$4 to $\simeq$3.7 to 3.8), coupled with increased coil current density, could solve this problem. If so, an ATFSR-size machine may be used for ignition demonstration or "multiplexed" (grouped with others) in a central station power complex.

Although the results of recent MHD stability and confinement studies have been used, it must be emphasized that the physics has been extended into an experimentally untried regime in which new phenomena are predicted (high beta through direct access to the second stability regime and an electron-dominated collisionless neoclassical transport regime). The goals of the existing experimental confinement program are to explore these issues and to provide a firmer footing for further studies.

For example, neoclassical ripple-induced losses of thermal particles have been used to evaluate a self-consistent radial electric field. However, nonambipolar anomalous losses or a nonthermal, anisotropic tail on either the electron or ion distribution function driven by auxiliary heating may dominate the particle losses and govern the potential (e.g., as shown by the Wendelstein VII-A beam injection experiments[12]). The choice of auxiliary heating (neutral beams, electron cyclotron resonant heating, ICRH, etc.) may well provide some external control of the ambipolar potential and therefore the confinement of thermal particles. This remains a rich area for both theoretical and experimental investigation.

ACKNOWLEDGMENT

This research was sponsored by the Office of Fusion Energy, U.S. Department of Energy, under contract DE-AC05-84OR21400 with Martin Marietta Energy Systems, Inc.

REFERENCES

1. J. F. LYON, B. A. CARRERAS, K. K. CHIPLEY, M. C. COLE, J. H. HARRIS, T. C. JERNIGAN, R. L. JOHNSON, V. E. LYNCH, B. E. NELSON, J. A. ROME, J. SHEFFIELD, and P. B. THOMPSON, "The Advanced Toroidal Facility," *Fusion Technol.*, **10**, 179 (1986).

2. B. A. CARRERAS, H. R. HICKS, J. A. HOLMES, V. E. LYNCH, L. GARCIA, J. H. HARRIS, T. C. HENDER, and B. F. MASDEN, "Equilibrium and Stability Properties of High-Beta Torsatrons," *Phys. Fluids*, **26**, 3569 (1983).

3. R. L. MILLER, "Recent Progress in Stellarator Reactor Conceptual Design," *Fusion Technol.*, **8**, 1581 (1985).

4. R. E. POTOK, D. R. COHN, and L. M. LIDSKY, "Design Features of T-2, A Torsatron Reactor with Continuous Coils," *Proc. 10th IEEE Symp. Fusion Engineering*, Philadelphia, Pennsylvania, Vol. 2, p. 1859, Institute of Electrical and Electronics Engineers (1983).

5. I. YANAGISAWA, N. UEDA, M. YAMADA et al., "A Design Study of a Heliotron Power Reactor," *Nucl. Technol./Fusion*, **4**, Part 3, 1302 (1983).

6. A. V. KOMIN, M. V. KRIVOSHEYEV, and A. B. MINEYEV, "Parameter Studies of a Stellarator Reactor with Various Types of Blankets," *Questions of Atomic Science and Technology Series: Thermonuclear Fusion*, Vol. 2, p. 12 (1984) (in Russian).

7. "UWTOR-M: A Conceptual Modular Stellarator Reactor," UWFDM-550, University of Wisconsin, Madison (1982).

8. R. L. MILLER, C. G. BATHKE, R. A. KRAKOWSKI et al., "Modular Stellarator Reactor Conceptual Design Study," *Nucl. Technol./Fusion*, **4**, Part 3, 1308 (1983).

9. J. T. LACATSKI, W. A. HOULBERG, and N. A. UCKAN, "Plasma Engineering Analysis of a Small Torsatron Reactor," ORNL/TM-9533, Oak Ridge National Laboratory (1985).

10. W. N. G. HITCHON, "Reduced-Aspect-Ratio Stellarator Reactors," *Nucl. Fusion*, **24**, 91 (1984).

11. D. E. HASTINGS, W. A. HOULBERG, and K. C. SHAING, "The Ambipolar Electric Field in Stellarators," *Nucl. Fusion*, **25**, 445 (1985).

12. WENDELSTEIN VII-A TEAM: G. CATTANEI, D. DORST, A. ELSNER, V. ERCKMANN, G. GRIEGER, P. GRIGULL, H. HACKER, H. J. HARTFUSS, M. A. HELLBERG, H. JÄCKEL, R. JAENICKE, J. JUNKER, M. KICK, H. KROISS, G. KUEHNER, H. MAASSBERG, C. MAHN, S. MARKLIER, G. MÜLLER, W. OHLENDORF, F. RAU, H. RENNER, H. RINGLER, F. SARDEI, M. TUTTER, A. WELLER, H. WOBIG, E. WÜRSCHING, M. ZIPPE, K. FREUDENBERGER, W. OTT, F.-P. PENNINGSFELD, E. SPETH, and H. BÜCHL, "Plasma Confinement and the Effect of Rotational Transform in the Wendelstein VII-A Stellarator," *Proc. 10th Int. Conf. Plasma Physics and Controlled Nuclear Fusion Research*, London, England, 1984, Vol. 2, p. 371, International Atomic Energy Agency, Vienna (1985).

13. C. C. BAKER et al., "STARFIRE: A Commercial Fusion Tokamak Power Plant Study," ANL/FPP-80-1, Argonne National Laboratory (1980).

14. J. H. HARRIS, Oak Ridge National Laboratory, Private Communication (1985).

15. J. SHEFFIELD, R. A. DORY, S. M. COHN, J. G. DELENE, L. PARSLY, D. E. T. F. ASHBY, and W. T. REIERSEN, "Cost Assessment of a Generic Magnetic Fusion Reactor," ORNL/TM-9311, Oak Ridge National Laboratory (1986).

16. R. SANDERS and I. N. SVIATOLAVSKY, "Divertor Target Design for the UWTOR-M Modular Stellarator Power Reactor," *Nucl. Technol./Fusion*, **4**, Part 3, 993 (1983).

17. W. A. HOULBERG, S. E. ATTENBERGER, and L. M. HIVELY, "Contour Analysis of Fusion Reactor Plasma Performance," *Nucl. Fusion*, **22**, 935 (1982).

18. K. C. SHAING, "Stability of the Radial Electric Field in a Nonaxisymmetric Torus," *Phys. Fluids*, **27**, 1567 (1984).

19. F. L. HINTON and R. D. HAZELTINE, "Theory of Plasma Transport in Toroidal Confinement Systems," *Rev. Mod. Phys.*, **48**, 239 (1976).

20. V. ERCKMANN, G. JANZEN, W. KASPAREK, G. MÜLLER, P. G. SCHÜLLER, K. SCHWÖRER, M. THUMM, R. WILHELM, and WENDELSTEIN VII-A TEAM, "Electron Cyclotron Resonance Heating Experiments in the Wendelstein VII-A Stellarator," *Fusion Technol.*, **7**, 275 (1985).

21. H. E. MYNICK and W. N. G. HITCHON, "Effect of the Ambipolar Potential on Stellarator Confinement," *Nucl. Fusion*, **23**, 1053 (1983).

22. L. M. KOVRIZHNYKH, "The Energy Confinement Time in Stellarators," *Nucl. Fusion*, **24**, 435 (1984).

23. D. E. HASTINGS, "Development of a Differential Equation for the Ambipolar Electric Field in a Bumpy Torus in the Low Collision Frequency Limit," *Phys. Fluids*, **27**, 2372 (1984).

24. K. C. SHAING, R. H. FOWLER, D. E. HASTINGS, W. A. HOULBERG, E. F. JAEGER, J. F. LYON, J. A. ROME, and J. S. TOLLIVER, "The Radial Electric Field in a Non-Axisymmetric Torus," *Proc. 10th Int. Conf. Plasma Physics and Controlled Nuclear Fusion Research*, London, England, 1984, Vol. 2, p. 189, International Atomic Energy Agency, Vienna (1985).